IEEE Photonics Journal
An IEEE Photonics Society Publication

Open Access

Superconducting Nanowire Single Photon Detector With Efficiency Over 60% for 2-μm-Wavelength

Volume 11, Number 6, December 2019

Hui Zhou
Yiming Pan
Lixing You
Hao Li
Yong Wang
Yan Tang
Heqing Wang
Xiaoyu Liu
Zhen Wang

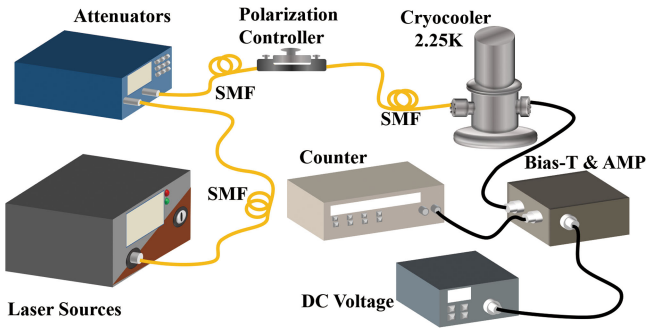

DOI: 10.1109/JPHOT.2019.2956755

IEEE photonics SOCIETY
IEEE

Superconducting Nanowire Single Photon Detector With Efficiency Over 60% for 2-μm-Wavelength

Hui Zhou,[1,2] **Yiming Pan**,[1,3] **Lixing You**,[1,2,4] **Hao Li**,[1,2,3] **Yong Wang**,[1] **Yan Tang**,[1,3] **Heqing Wang**,[1,3] **Xiaoyu Liu**,[1,2] **and Zhen Wang**[1,2]

[1]State Key Laboratory of Functional Materials for Informatics, Shanghai Institute of Microsystem and Information Technology, Chinese Academy of Sciences, Shanghai 200050, China
[2]CAS Center for Excellence in Superconducting Electronics, Shanghai 200050, China
[3]University of Chinese Academy of Sciences, Beijing 100049, China
[4]Center of Materials Science and Optoelectronics Engineering, University of Chinese Academy of Sciences, Beijing 100049, China

DOI:10.1109/JPHOT.2019.2956755

Manuscript received August 13, 2019; revised November 12, 2019; accepted November 26, 2019. Date of publication November 29, 2019; date of current version December 17, 2019. This work was supported in part by the National Key R&D Program of China under Grant 2017YFA0304000, in part by the National Natural Science Foundation of China under Grants 61971408, 61827823 and 61671438, and in part by the Program of Shanghai Academic/Technology Research Leader under Grant 18XD1404600. Corresponding author: Lixing You (e-mail: lxyou@mail.sim.ac.cn).
This article has supplementary downloadable material available at http://ieeexplore.ieee.org, provided by the authors.

Abstract: We demonstrate superconducting nanowire single photon detector (SNSPD) for the wavelength at around 2 μm. The linewidth of the NbN nanowire is squeezed to 56 nm to increase the intrinsic response efficiencies at longer wavelengths such as 2 μm. Serially connecting avalanche architecture is applied to increase the signal-to-noise ratio (SNR) of the response signal. Further, the optical cavity is optimized to improve the absorption of the device. A silica single-mode fiber is adopted to introduce photons to the SNSPD at a temperature of 2.25 K using a Gifford–McMahon cryocooler. The SNSPD exhibits detection efficiencies of 58%, 67%, and 63% at wavelengths of 1550, 1700, and 2000 nm, respectively, with dark count rate of $\sim$12 kcps, which is reduced to 2 cps when the attached fiber pigtail is all placed inside the 40-K cryostat. The detection efficiency at 2000 nm is 2.5 times greater than that of the best previously developed detector with an efficiency of 25%. Our SNSPD is promising for practical applications in molecular science and earth meteorology.

Index Terms: Photon detectors, superconducting nanowire single photon detectors (SNSPDs), system detection efficiency, 2-μm-wavelength.

1. Introduction

Superconducting nanowire single photon detectors (SNSPDs) demonstrate a low dark count rate, minimal timing jitter, short reset time, and near unity detection efficiency in the visible-to-near-infrared spectral range. They outperform other single-photon detectors (SPDs) such as Si and InGaAs avalanche photodiodes (APDs) and vacuum photomultipliers (PMTs). SNSPDs are particularly well-suited for applications at telecom wavelengths in the context of long-haul quantum

key distribution [1], quantum random number generation [2], and satellite laser ranging [3]–[5]. Nowadays, emerging mid-infrared applications in environmental gas monitoring and life sciences require SPDs with better mid-infrared sensitivity and temporal resolution [6], [7]. Such applications include molecular science [8], earth meteorology [9], remote sensing [10], and human breath analysis [11].

SNSPDs fabricated via superconducting materials with gap energies in $\sim$meV are natural broadband detectors and function in both visible and infrared wavelengths (including wavelengths longer than 1.8 μm, which is the limit for InGaAs APDs). Marsili *et al.* have reported SNSPDs made of polycrystalline niobium nitride (NbN) nanowires that exhibited detection efficiencies of about 2.6%–5.5% with an intrinsic dark count rate (DCR) of about 15 cps at wavelengths ranging from 0.5 to 5 μm [12]. Recently, Divochiy *et al.* demonstrated that using disordered NbN films they improved system detection efficiencies (SDEs) to 60% at 1700 nm, 25% at 2000 nm, and 15% at 2300 nm with a DCR of about 250 cps [13]. With amorphous tungsten silicide (WSi), the single photon sensitivity of SNSPD was demonstrated up to 7 μm in a laser-induced fluorescence experiment [8]. These works experimentally demonstrated the responding capability of SNSPDs at longer wavelengths. Although SNSPDs with SDEs over 90% at 1550 nm [14], [15] and shorter wavelengths [16], [17] have been reported, few studies with modest SDE have focused on SNSPDs targeting the wavelengths beyond 1.5 μm [12], [13].

Herein, an NbN SNSPD was fabricated and optimized for wavelengths up to 2000 nm. Several methods were adopted to improve the SDE: First, the linewidth of the nanowire was reduced to 56 nm to increase the intrinsic detection efficiency (IDE) for longer wavelengths. Additionally, a serially connecting avalanche architecture [18], [19] was designed to increase the signal-to-noise-ratio (SNR) of the response signal. Finally, an optimized optical cavity was implemented to improve the absorptance. The SDEs reach 58%, 67% and 63% for the wavelengths of 1550, 1700 and 2000 nm at the DCR of $\sim$12 kcps, respectively. The high efficiency single photon detector at 2000 nm is appealing for various applications, such as overtone spectroscopy of H_2O clusters [20], [21], earth meteorology of cloud characteristic invers [22], high-resolution characterization of quantum dots [23] and remote sensing Lidar [10], [24].

2. Device Design and Fabrication

To obtain high-SDE SNSPDs that are suitable for longer wavelengths, both high absorptance and high IDE are required. The former can be easily achieved by optimizing the parameters of the optical structures. Further, it is easier to get a higher IDE for longer wavelengths using WSi SNSPDs than Nb(Ti)N SNSPDs because WSi has a lower gap energy than Nb(Ti)N. However, WSi SNSPDs usually work at sub-Kelvin temperature that burdens the cryogenics for practical applications. Nb(Ti)N based SNSPDs are more economical choices for longer wavelengths since they can work with a compact 2-stage mechanical cryocooler, and it is necessary to reduce the linewidth of the nanowire to improve the IDE of the device as described previously [12].

The schematic of our proposed SNSPD is showing in Fig. 1(a). The layers, from top to bottom, are Au/Ti, SiO, NbN, and double-sided thermally oxidized Si as the substrate. A metallic mirror with a layer of SiO was placed atop the nanowires and a SiO_2/Si layer was placed beneath the nanowires to form an optical cavity; this design was expected to enhance the absorption of the nanowires when the SNSPD was illuminated from the backside of the substrate. The SiO_2 layer in the bottom works as an anti-reflection coating for increased optical transmission. Here, 1850 nm was selected as the center wavelength to obtain a relatively high absorptance over the band of 1550–2200 nm. The thicknesses of the SiO_2 and SiO layers were about one-quarter of the targeted wavelength to facilitate the resonant absorption.

The refractive index of NbN at approximately 1850 nm was $n_{NbN} = 6.87 + 6.13i$, measured using a spectroscopic ellipsometer (IR-VASE Mark II, J.A. Woollam) on a 30-nm-thick NbN film. The refractive indices of the other materials used in the detector design at the same wavelength are $n_{Au} = 0.77 + 12.7i$ [25], $n_{SiO} = 1.86$, $n_{Si} = 3.43$, and $n_{SiO_2} = 1.44$. To obtain a high IDE at a relatively long wavelength, the thickness, width, and pitch of the NbN nanowires were selected to be 6, 60,

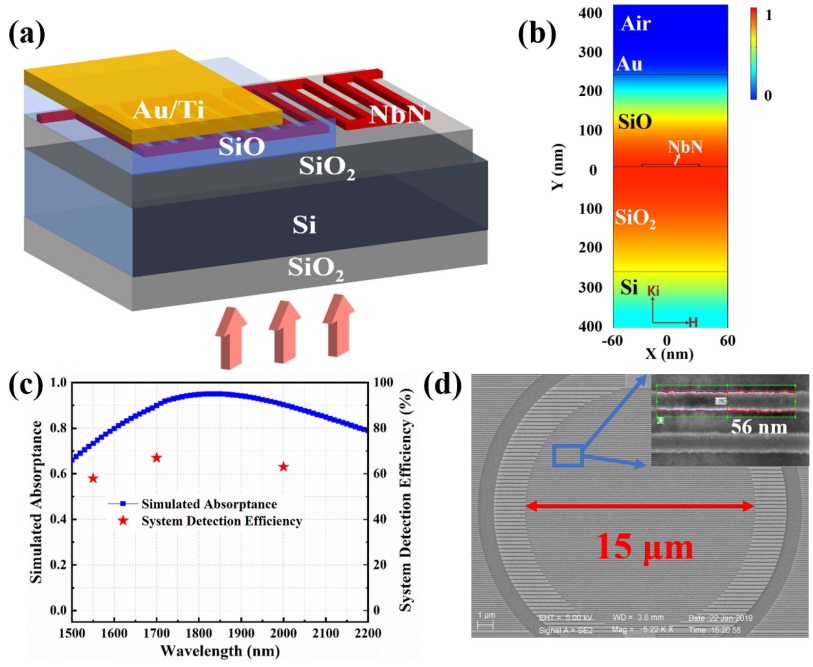

Fig. 1. (a) Schematics of the device (not to scale), where 2 nanowires are connected in parallel to improve the signal-to-noise-ratio. (b) Electric field intensity distribution when TE waves are incident on the nanowire from the back of the substrate. (c) Simulated absorptance (blue square line) and the measured SDE as a function of the wavelength (red stars). (d) SEM image of the SNSPD (top view), indicating the active area with a diameter of 15 μm; The nanowire has a width of 56 $\pm$ 2.7 nm (see the inset), which was slightly smaller than the designed value of 60 nm.

and 120 nm, respectively. A serially connecting avalanche architecture is applied to improve the SNR of the response pulse [18].

An electromagnetic simulation was performed using Comsol Multiphysics [26] considering that a plane wave incident on the detector. The detector is modeled as a two-dimensional infinitely extended periodic grating in the horizontal direction and therefore neglects any edge effects of the real meander. Floquet boundary conditions and Port conditions are applied in the horizontal and longitudinal direction, respectively. Fig. 1(b) shows the electric field intensity for light waves with electric field parallel to the nanowire (TE waves). Note that the nanowire is located at the antinode of the cavity field which accounts for the high optical absorption as expected. As shown in Fig. 1(c), the simulated absorptance of the device exceeds 73% in the wavelength range of 1550–2200 nm, indicating potential high SDEs over this wavelength range. The maximum absorption is 95% at the wavelength of 1850 nm and the absorption is 90% at the wavelength of 2000 nm.

The device was fabricated as follows. A 6-nm NbN thin film with a sheet resistance of 489 Ω at 20 K was first deposited onto a double-sided thermally oxidized Si substrate via reactive dc-magnetron sputtering in an Ar/N_2 gas mixture at room temperature under a total pressure of 0.27 Pa (the partial pressures of Ar and N_2 were 79% and 21%, respectively). The film was coated with an electron-beam photoresist, PMMA, which was patterned using electron-beam lithography to form the nanowire structure and subsequently etched via reactive-ion etching in CF_4 plasma. Several tens of parallel pairs of 60 nm-wide nanowires were connected in series, covering a sensitive area of 15 μm in diameter as shown in the scanning electron microscopy (SEM) image in Fig. 1(d). An analysis of the SEM images using ProSEM revealed that the line edge roughness was about LER $= 3 * \sigma = 2.7$ nm, where σ is the standard deviation of the feature edge; this measurement suggests that the nanowires exhibited good uniformity. Then, a 50 Ω-matched coplanar waveguide was formed using ultraviolet lithography and reactive-ion etching. A 235 nm-thick SiO dielectric

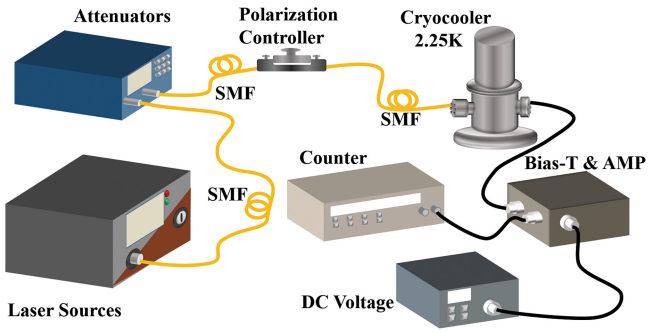

Fig. 2. Schematics of system for characterizing the SNSPD (SMF: single-mode fiber; AMP: amplifier).

layer and a 5 nm/100 nm-thick Ti/Au mirror were formed via e-beam evaporation atop the nanowires to enhance the light absorption. The superconducting transition temperature (T_c) of the detector, which is defined as the midpoint of the resistivity–temperature transition, was measured to be 7.7 K.

3. Measurement

The fabricated device was packaged in a copper sample mount. To ensure efficient optical coupling, a single-mode optical fiber with GRIN lenses (SMFL) was positioned at the backside of the device. The 1700-nm laser was chosen for the alignment check, using a homemade alignment system based on an inverted microscope to ensure that the focused beam spot of the incident light was smaller than the sensitive area. The silica single-mode fiber (SMF) provides good transmission for photons with wavelengths from the visible range up to 2200 nm [27]. However, SMF has a high bend-loss sensitivity at a wavelength of 2000 nm; therefore, bending of the fiber during optical connecting was avoided as much as possible. The packaged module was then mounted on the cold head of a two-stage Gifford–McMahon cryocooler set to a working temperature of 2.25 K. The device was connected to a room-temperature bias-tee outside the cryocooler. Bias current was supplied to the device by a voltage source in series with a 100 kΩ resistor via the dc port of the bias-tee. The voltage pulses generated by the SNSPD were transferred to rf port of the bias-tee and amplified using a room-temperature 50 dB low-noise amplifier (RF Bay Inc. LNA-650). The amplified pulse signals were either read by an oscilloscope or counted by a photon counter.

The device performance was experimentally characterized at three different wavelengths: 1550, 1700, and 2000 nm. Fig. 2 shows the setup used for the measurements. The polarized laser pulses at 1550 and 1700 nm were generated by a supercontinuum laser (NKT: EXB-3) with an acousto-optic tunable filter (NKT: SuperK SELECT). The 2000 nm laser pulses were generated by a thulium-doped fiber laser (Thorlabs: LFL2000) connected with an in-line fiber polarizer, which has a signal-to-noise ratio of about 80 dB in spectrum (600–2000 nm), indicating the influence of signals of other wavelengths from the laser was negligible. Two attenuators (81570As, Keysight) were used in the 1550–1700 nm measurement, and as for 2000 nm, a custom-made attenuator (LQ-VOA-2000, QOPTRONICS) was added to the system (details can be found in the supplementary information). Here, two power meters were utilized: a Keysight 81634B was used to calibrate the wavelengths from 1550 to 1700 nm and a Thorlabs Energy Meter PM100D with an integrating sphere photodiode power sensor (S148C) was used to calibrate the wavelength of 2000 nm. Because the attenuators are sensitive to the wavelength, the actual attenuation for each wavelength was calibrated using the power meter. The light polarization was manipulated using a squeeze-type polarization controller (Thorlabs: PLC900). To conduct each measurement, the input laser (i.e., the photon source) was heavily attenuated to a photon flux of 10^6 photons/s using the variable attenuators. The SDE is defined as (OPR$-$DC)/PR, where OPR is the output photon rate of an SNSPD (as recorded with a photon counter), DC represents the dark count when the laser is blocked, and PR is the total photon input rate to the system. At each bias current, the OPR and DC were each collected for

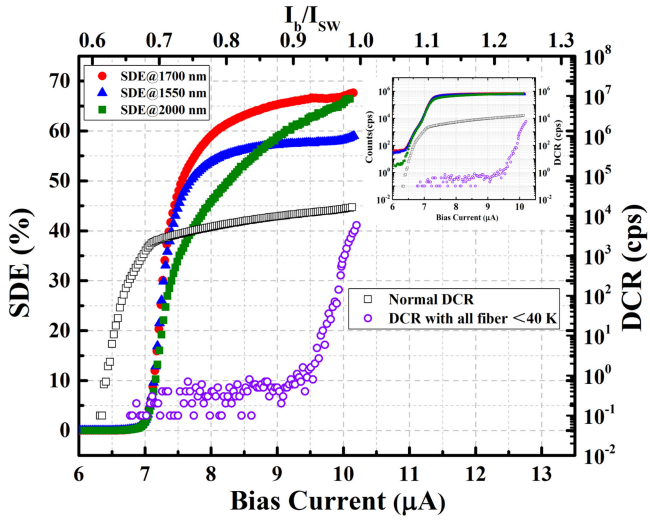

Fig. 3. SDE and DCR as functions of the bias current at various wavelengths (indicated by different colors). Inset shows the results when light counts and DCR are plotted in the same logarithmic scale.

10 s. The total errors were calculated to be 2.82% and 5.1% for 1550–1700 nm and 2000 nm, respectively (details on the error estimation can be found in the supplementary information), which is calculated as $Total\ error = \sqrt{error^2_{powermeter} + error^2_{attenuators} + error^2_{laser}}$.

Fig. 3 shows the SDE and DCR as functions of the bias current. The avalanche current for the SNSPD was about $0.67I_{sw}$, where I_{sw} is the switching current of the detector. The SDEs at 1550, 1700, and 2000 nm reached up to 58%, 67%, and 63%, respectively, with a dark count rate of about 12 kcps; the corresponding absorptance values were calculated to be 73%, 90%, and 90%, respectively.

The observed trend in the measured SDE at different wavelengths was consistent with the simulation results shown in Fig. 1(c). It can be extrapolated that the SDE at a wavelength of 2200 nm would be up to about 50% based on the trend observed in the simulation. However, it is improper since the triggering probability of SNSPD is less than unity due to the smaller photon energy. To obtain a higher SDE at longer wavelengths, one needs to further squeeze the width of the nanowire or the film thickness and optimize the optical cavity design.

Since no measures were put in place to suppress the dark counts of this system, the dark counts were relatively high (Fig. 3 (black hollow squares)); this was attributed to the black-body radiation from the optical fiber, which propagates through the fiber. Indeed, the measured DCR increases rapidly simultaneously with the increase of SDE and the plateau of DCR seems steeper than measured light counts, which is evident if both DCR and light counts are plotted in the same logarithmic scale (see the inset of Fig. 3). Moreover, the avalanche currents for light counts and dark counts appear at around the same bias current of 6.3 μA. To further verify the origin of DCR, the SMF pigtail was placed inside the first stage of the cryocooler with the temperature below 40 K, the DCR was significantly reduced (Fig. 3 (purple hollow circles)). For practical applications, various filtering techniques can be adopted to reduce the DCR; e.g., placing a band-pass filter (BPF) at 3 K [28], integrating the BPF on the substrate [29], or on the end-face of the coupling fiber [30].

To examine the speed of the device, the waveform and count rate (CR) of the detector were measured as shown in Fig. 4(a). The measured oscilloscope single shot trace of the real-time photon response pulse shown in the inset of Fig. 4(a), indicates that the recovery time (defined as the time width at 1/e = 0.368 of the maximum pulse amplitude), was 12.4 ns as given by the exponential fitting of the falling edge. Additionally, the CR dependence of the normalized SDE at a wavelength of 1550 nm was evaluated by increasing the incident photon intensity. The bias current

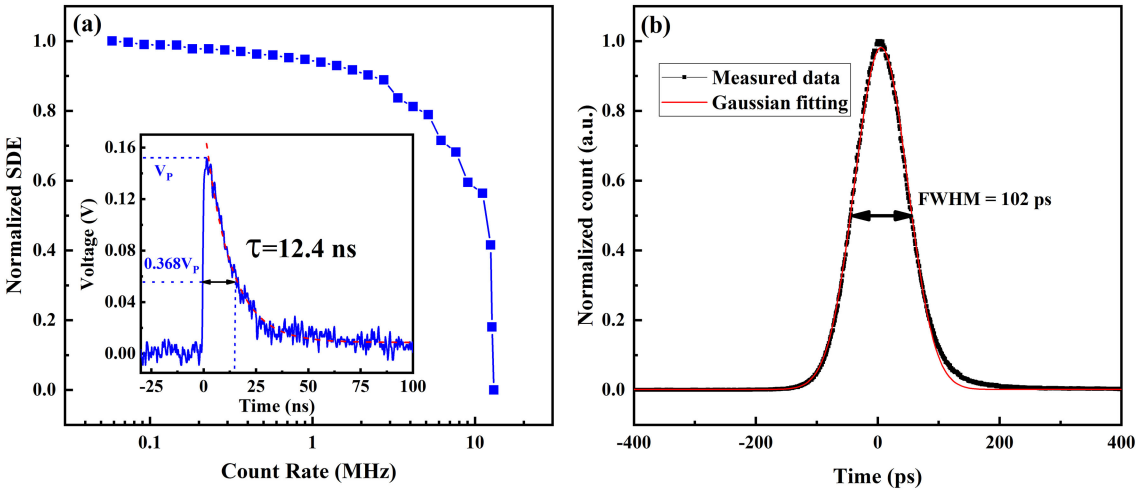

Fig. 4. (a) Response counting rate dependence of the normalized SDE measured at a wavelength of 1550 nm. Inset: Oscilloscope map of the response at a bias current of 9.5 μA. The exponential fitting of the falling edge is displayed as red dashed line. (b) Histogram of the time-correlated photon counts measured at a wavelength of 1550 nm (black) and the Gaussian distribution that was fitted to the data (red).

was initially set at $0.95I_{sw}$. The SDE remained nearly constant as the CR increased from 0.1 to 1 MHz, but decreased significantly as the CR continued to increase to higher rates because the detector could not respond to all of the incoming photons. The CR reached about 12 MHz before the SDE decreased to 1/e of its maximum value. The maximal count rate of the device is limited by the recovery time of nanowire and/or the readout circuit. Thus, to further improve the CR, the kinetic inductance of SNSPD could be decreased or the readout circuits could be optimized using, e.g., a DC-coupled readout circuit [31] or a resistive network [32].

Finally, the timing jitter of the SNSPD system was measured via the time-correlated single-photon counting method using a femtosecond laser at a wavelength of 1550 nm [33]. The timing jitter, which is defined as the full width at half maximum (FWHM) value of the histogram of the time-correlated photon counts, was 102 ps (Fig. 4(b)).

4. Conclusions

In conclusion, we demonstrated NbN SNSPD designed for wavelengths up to 2000 nm. The SDE reached 58%, 67%, and 63% for wavelengths of 1550, 1700, and 2000 nm, respectively. There is still room for further improving the SDE and further extending to longer wavelengths. SNSPDs with high SDE at longer wavelengths is useful for various infrared applications.

References

[1] H.-L. Yin *et al.*, "Measurement-device-independent quantum key distribution over a 404 km optical fiber," *Phys. Rev. Lett.*, vol. 117, no. 19, 2016, Art. no. 190501.
[2] Y. Liu *et al.*, "Device-independent quantum random-number generation," *Nature*, vol. 562, no. 7728, pp. 548–552, 2018.
[3] H. Li *et al.*, "Superconducting nanowire single photon detector at 532 nm and demonstration in satellite laser ranging," *Opt. Express*, vol. 24, no. 4, pp. 3535–3542, 2016.
[4] L. Xue *et al.*, "Satellite laser ranging using superconducting nanowire single-photon detectors at 1064 nm wavelength," *Opt. Lett.*, vol. 41, no. 16, pp. 3848–3851, 2016.
[5] R. Tang *et al.*, "Light curve measurements with a superconducting nanowire single-photon detector," *Opt. Lett.*, vol. 43, no. 21, pp. 5488–5491, 2018.
[6] M. N. Abedin, M. G. Mlynczak, and T. F. Refaat, "Infrared detectors overview in the short-wave infrared to far-infrared for CLARREO mission," in *Proc. Infrared Remote Sens. Instrum. XVIII*, 2010, Paper 78080V.

[7] S.-S. Kim, C. Young, B. Vidakovic, S. G. Gabram-Mendola, C. W. Bayer, and B. Mizaikoff, "Potential and challenges for mid-infrared sensors in breath diagnostics," *IEEE Sens. J.*, vol. 10, no. 1, pp. 145–158, Jan. 2010.
[8] L. Chen *et al.*, "Mid-infrared laser-induced fluorescence with nanosecond time resolution using a superconducting nanowire single-photon detector: New technology for molecular science," *Accounts Chem. Res.*, vol. 50, no. 6, pp. 1400–1409, 2017.
[9] J. Li, U. Parchatka, R. Königstedt, and H. Fischer, "Real-time measurements of atmospheric CO using a continuous-wave room temperature quantum cascade laser based spectrometer," *Opt. Express*, vol. 20, no. 7, pp. 7590–7601, 2012.
[10] R. Targ *et al.*, "Coherent lidar airborne wind sensor II: Flight-test results at 2 and 10 μm," *Appl. Opt.*, vol. 35, no. 36, pp. 7117–7127, 1996.
[11] G. Song *et al.*, "Quantitative breath analysis of volatile organic compounds of lung cancer patients," *Lung Cancer*, vol. 67, no. 2, pp. 227–231, 2010.
[12] F. Marsili *et al.*, "Efficient single photon detection from 500 nm to 5 μm wavelength," *Nano Lett.*, vol. 12, no. 9, pp. 4799–4804, 2012.
[13] A. Divochiy *et al.*, "Single photon detection system for visible and infrared spectrum range," *Opt. Lett.*, vol. 43, no. 24, pp. 6085–6088, 2018.
[14] W. Zhang *et al.*, "NbN superconducting nanowire single photon detector with efficiency over 90% at 1550 nm wavelength operational at compact cryocooler temperature," *Sci. China Phys., Mech. Astron.*, vol. 60, no. 12, 2017, Art. no. 120314.
[15] F. Marsili *et al.*, "Detecting single infrared photons with 93% system efficiency," *Nat. Photon.*, vol. 7, no. 3, 2013, Art. no. 210.
[16] K. Smirnov *et al.*, "NbN single-photon detectors with saturated dependence of quantum efficiency," *Supercond. Sci. Technol.*, vol. 31, no. 3, 2018, Art. no. 035011.
[17] K. Erotokritou *et al.*, "Nano-optical photoresponse mapping of superconducting nanowires with enhanced near infrared absorption," *Supercond. Sci. Technol.*, vol. 31, no. 12, 2018, Art. no. 125012.
[18] S. Miki, M. Yabuno, T. Yamashita, and H. Terai, "Stable, high-performance operation of a fiber-coupled superconducting nanowire avalanche photon detector," *Opt. Express*, vol. 25, no. 6, pp. 6796–6804, 2017.
[19] M. Ejrnaes *et al.*, "Large signal amplitude and bias range of cascade switch superconducting nanowire single photon detectors," *IEEE Trans. Appl. Supercond.*, vol. 19, no. 3, pp. 323–326, Jun. 2009.
[20] M. Falk, and T. A. Ford, "Infrared spectrum and structure of liquid water," *Can. J. Chem.*, vol. 44, no. 14, pp. 1699–1707, 1966.
[21] S. A. Nizkorodov, M. Ziemkiewicz, D. J. Nesbitt, and A. E. W. Knight, "Overtone spectroscopy of H2O clusters in the vOH $=$ 2 manifold: Infrared-ultraviolet vibrationally mediated dissociation studies," *J. Chem. Phys.*, vol. 122, no. 19, 2005, Art. no. 194316.
[22] J. Wang, C. Liu, M. Min, X. Hu, Q. Lu, and L. Husi, "Effects and applications of satellite radiometer 2.25 um channel on cloud property retrievals," *IEEE Trans. Geosci. Remote Sens.*, vol. 56, no. 9, pp. 5207–5216, Sep. 2018.
[23] D. Elvira *et al.*, "Time-resolved spectroscopy of InAsP/InP(001) quantum dots emitting near 2 μm," *Appl. Phys. Lett.*, vol. 97, no. 13, 2010, Art. no. 131907.
[24] Y. J. Kaufman *et al.*, "The MODIS 2.1-μm channel-correlation with visible reflectance for use in remote sensing of aerosol," *IEEE Trans. Geosci. Remote Sens.*, vol. 35, no. 5, pp. 1286–1298, Sep. 1997.
[25] P. B. Johnson and R. W. Christy, "Optical constants of the noble metals," *Phys. Rev. B*, vol. 6, no. 12, pp. 4370–4379, 1972
[26] H. Li *et al.*, "Large-sensitive-area superconducting nanowire single-photon detector at 850 nm with high detection efficiency," *Opt. Express*, vol. 23, no. 13, pp. 17301–17308, 2015.
[27] P. S. Kuo, "Using silica fiber coupling to extend superconducting nanowire single-photon detectors into the infrared," *OSA Continuum*, vol. 1, no. 4, pp. 1260–1266, 2018.
[28] H. Shibata, K. Shimizu, H. Takesue, and Y. Tokura, "Superconducting nanowire single-photon detector with ultralow dark count rate using cold optical filters," *Appl. Phys. Express*, vol. 6, no. 7, 2013, Art. no. 072801.
[29] X. Y. Yang *et al.*, "Superconducting nanowire single photon detector with on-chip bandpass filter," *Opt. Express*, vol. 22, no. 13, pp. 16267–16272, 2014.
[30] W. J. Zhang *et al.*, "Fiber-coupled superconducting nanowire single-photon detectors integrated with a bandpass filter on the fiber end-face," *Supercond. Sci. Technol.*, vol. 31, no. 3, 2018, Art. no. 035012.
[31] A. J. Kerman, D. Rosenberg, R. J. Molnar, and E. A. Dauler, "Readout of superconducting nanowire single-photon detectors at high count rates," *J. Appl. Phys.*, vol. 113, no. 14, 2013, Art. no. 144511.
[32] Q. Y. Zhao *et al.*, "Counting rate enhancements in superconducting nanowire single-photon detectors with improved readout circuits," *Opt. Lett.*, vol. 39, no. 7, pp. 1869–1872, 2014.
[33] L. You *et al.*, "Jitter analysis of a superconducting nanowire single photon detector," *AIP Adv.*, vol. 3, no. 7, 2013, Art. no. 072135.